Title: Modeling long-term salt marsh response to sea level rise in the sediment-deficient Plum Island Estuary, MA

Authors: Amy K. Langston[1*], Orencio Durán Vinent[1, 2], Ellen R. Herbert[1, 3], Matthew L. Kirwan[1]

[1]Virginia Institute of Marine Science, William & Mary, PO Box 1346, Gloucester Point, VA, USA 23062

[2]Department of Ocean Engineering, Texas A&M University, College Station, TX, USA 77843

[3]Ducks Unlimited, Memphis, TN, USA 38129

Co-author emails: oduranvinent@exchange.tamu.edu; eherbert@ducks.org; kirwan@vims.edu

*corresponding author: (804) 684-7592; aklangston@vims.edu

Running head: Salt marsh response to sea level rise

Keywords: accretion, elevation capital, low marsh, high marsh, suspended sediment concentration

Abstract

An accelerating global rate of sea level rise, coupled with direct human impacts to coastal watersheds and shorelines, threatens the continued survival of salt marshes. We developed a new landscape-scale numerical model of salt marsh evolution and applied it to marshes in the Plum Island Estuary (Massachusetts, USA), a sediment-deficient system bounded by steep uplands. To capture complexities of vertical accretion across the marsh platform, we employed a novel approach that incorporates spatially variable suspended sediment concentrations and biomass of multiple plant species as functions of elevation and distance from sediment sources. The model predicts a stable areal extent of Plum Island marshes for a variety of sea level rise scenarios through 2100, where limited marsh drowning is compensated by limited marsh migration into adjacent uplands. Nevertheless, the model predicts widespread conversion of high marsh vegetation to low marsh vegetation, and accretion deficits that indicate eventual marsh drowning. Although sediment-deficient marshes bounded by steep uplands are considered extremely vulnerable to sea level rise, our results highlight that marshes with high elevation capital can maintain their areal extent for decades to centuries even under conditions in which they will inevitably drown.

35 Introduction

36 Coastal salt marshes occupy a precarious position in the landscape, linking land and sea
37 in temperate latitudes along low-energy, gently-sloped coastlines. Within this setting they
38 sequester carbon, cycle nutrients, provide habitat, stabilize shorelines, and buffer waves and
39 storms (Zedler and Kercher 2005). Subject to hydrodynamics that dictate their geomorphology,
40 salt marshes persist via biophysical feedbacks between sediment accumulation, primary
41 productivity, and sea level change (Redfield 1972; Friedrichs and Perry 2001; Morris et al.
42 2002). However, during the past century, the global mean rate of sea level rise (SLR) has
43 increased from 1.7 mm y^{-1} (1900-1990) to a current rate of 3.3 mm y^{-1} since 1993 (IPCC 2013;
44 Wright et al. 2019). Projected global increases may exceed 15 mm y^{-1} by the end of the century,
45 depending on future greenhouse gas emissions, and local rates in many regions may increase
46 even faster (IPCC 2013; Horton et al. 2014; Nerem et al. 2018; Bamber et al. 2019). While salt
47 marshes have largely survived changes in sea level over the past 4,000 years, an accelerating
48 global rate of SLR jeopardizes the ability of marshes to maintain dynamic equilibrium with sea
49 level (Kirwan and Megonigal 2013).

50 Recent observations of marsh submergence have prompted concern for salt marsh
51 persistence worldwide (e.g., Reed 1995; FitzGerald et al. 2008; Kirwan and Megonigal 2013;
52 Crosby et al. 2016). Extensive marsh loss from subsidence, accretion deficits, and human
53 impacts has occurred in the world's largest estuaries, including the Mississippi River Delta,
54 Yellow River Delta, and Venice Lagoon (Carniello et al. 2009; Murray et al. 2014; Jankowski et
55 al. 2017; Gu et al. 2018). However, several marshes in northwest Europe and North America
56 have shown resilience to SLR (French 2006; Kirwan et al. 2016a). The global extent of marshes
57 predicted by 2100 is widely variable: estimates range from 30% loss to 60% gain, depending on

58 available migration space (Schuerch et al. 2018; Rogers et al. 2019). Varying responses to SLR
59 create a need for predictive models that evaluate salt marsh outcomes based on local conditions
60 and under different SLR scenarios to inform strategies that can minimize future loss.
61 Coastal salt marshes naturally maintain stability relative to sea level through non-linear
62 ecogeomorphic feedbacks that influence vertical accretion and landward transgression (Redfield
63 1972; Friedrichs and Perry 2001; Morris et al. 2002; Mudd et al. 2009; Fagherazzi et al. 2012;
64 Kirwan and Megonigal 2013; FitzGerald and Hughes 2019). Tidal flooding drives the
65 accumulation of mineral sediments and organic material that contribute to marsh elevation gain.
66 Tidal waters deliver mineral sediments to the marsh surface during periods of inundation. Marsh
67 vegetation facilitates sediment deposition by slowing water velocities and trapping sediment, and
68 also supplies organic matter that contributes to elevation gain (Gleason et al. 1979; Nyman et al.
69 2006; Li and Yang 2009). Rates of sediment deposition and primary productivity vary spatially
70 across a marsh, depending on surface elevation relative to sea level and distance from tidal
71 channels delivering sediment (Kirwan and Guntenspergen 2012; Schalles et al. 2013; Swanson et
72 al. 2014; Roner et al. 2016). Because non-linear dynamics of mineral and organic accretion are
73 fundamental to marsh evolution and resilience, it is critical that predictive models incorporate
74 them when evaluating marsh response to SLR.
75 Marsh accretion rates tend to increase with flooding frequency so that marshes generally
76 adapt to changes in SLR rates as long as surface elevations remain within the range required for
77 plant survival (Morris et al. 2002; Cadol et al. 2014; Kirwan et al. 2016a). Marsh loss is also
78 mitigated by lateral migration induced by SLR. Increased tidal inundation and salinity promote
79 landward marsh encroachment into upland areas unencumbered by topographic or anthropogenic
80 barriers (e.g., steep slopes, shoreline protection structures, urban development; Kirwan et al.

2016a; b; Langston et al. 2017; Schieder et al. 2018; Borchert et al. 2018; Kirwan and Gedan 2019). For marshes unable to keep pace vertically with SLR, landward migration is essential for survival (Schuerch et al. 2018). When upland marsh migration is restricted, marshes are subjected to coastal squeeze where lateral erosion results in loss of marsh area (Torio and Chmura 2013; Kirwan et al. 2016b; Thorne et al. 2018).

Marsh loss is most dramatic in regions where natural feedbacks between vertical accretion and SLR have been disrupted and/or landward transgression restricted (Kennish 2001; Kearney et al. 2002; Gittman et al. 2015). Human disturbances, including the construction of dams and reservoirs, afforestation, soil conservation, and agricultural sediment control practices disrupt feedbacks between marsh elevation and sea level by reducing sediment delivery (Kennish 2001; Kirwan and Megonigal 2013; Weston 2014). Damming of rivers is a major cause of reduced sediment supply to coastal marshes that has resulted in marsh loss worldwide (Syvitski et al. 2005). Likewise, topographic and anthropogenic barriers cause marsh loss by limiting landward retreat (Doody 2013; Torio and Chmura 2013; Kirwan et al. 2016b; Enwright et al. 2016). While much work has been done assessing general salt marsh responses to SLR, more work is needed to evaluate whether marshes with reduced sediment inputs and limited room for landward migration can survive SLR.

Predicting responses of marshes to SLR is challenging because complex interactions between tidal flooding, plant productivity, and sediment transport processes drive long-term behavior of coastal salt marshes (Kirwan et al. 2010; Kirwan and Megonigal 2013). Spatially resolved, landscape-scale models of salt marsh evolution tend to fall into one of two categories. One category emphasizes ecogeomorphic connectivity between channels and the marsh platform (e.g., D'Alpaos et al. 2007; Kirwan and Murray 2007; Temmerman et al. 2007). These models

tend to be developed to explore general behavior or to make predictions for a single location, and rely on relatively complex parameterizations for the flow of water and sediment across the model domain. A second category of models emphasizes vertical accretion on the marsh platform itself (e.g., Swanson et al. 2014; Schile et al. 2014; Alizad et al. 2016a; Cadol et al. 2016; Wu et al. 2017; Thorne et al. 2018). These point-based models simplify spatial connectivity, and allow for easier parameterization and application to multiple sites. The most prominent point-based models (e.g. SLAMM, MEM, WARMER) can simulate the dynamic interaction between flooding frequency and vertical accretion but neglect lateral sediment transport across the marsh (D'Alpaos and Marani, 2013), which leads to sediment deposition rates that depend only on marsh elevation.

Here, we propose a new, spatially resolved, landscape-scale model of salt marsh vertical accretion that accounts for lateral suspended sediment transport, as well as organic matter production of multiple plant species. We used the model to predict salt marsh response to SLR at the Plum Island Ecosystems (PIE) Long-Term Ecological Research Site (LTER; MA, USA). This location is sediment-limited and bounded by steep uplands that limit marsh transgression. Given these constraints, we expected PIE marshes would be especially vulnerable to drowning under accelerated SLR but found that their initially high elevations allowed them to persist with no loss in areal extent through 2100.

Methods

Study site

The PIE LTER is a 60-km^2 estuary that supports approximately 40 km^2 of salt marsh, making it the largest remaining area of intertidal salt marshes in the northeastern US (Kirwan et al. 2011; Fig. 1). The marsh expanded rapidly during the 18th and 19th centuries when

deforestation increased sediment delivery to the coast following European settlement (Kirwan et al. 2011). The estuary is macrotidal and has a tidal range of 2.9 m. External sediment is supplied by the ocean and three major rivers: Parker, Ipswich, and Rowley, all of which are dammed. Median suspended sediment concentration is approximately 15 mg L^{-1} and varies across the estuary; at the head of the estuary it falls below 10 mg L^{-1} and reaches 40 mg L^{-1} at the mouth (Hopkinson et al. 2018). The majority of the PIE landscape is composed of high marsh (mean elevation of 1.38 m above MSL) dominated by *Spartina patens*; low marsh (mean elevation of 0.98 m above MSL), dominated by tall form *S. alterniflora*, accounts for ~10% of total salt marsh area (including ponds; Wilson et al. 2014). The local long-term (1921-2018) mean rate of SLR is approximately 2.83 mm y^{-1}, based on the sea level trend at the Boston tide station (#8443970). In recent decades (1990-2018) the rate has increased to approximately 4.80 mm y^{-1}. Marshes at PIE are currently in dynamic equilibrium with the long-term rate of SLR, manifested by a cyclical pattern of pond formation and marsh recovery (Wilson et al. 2014), and mineral accretion supplemented by sediment from channel edge erosion (Hopkinson et al. 2018).

Model description

We developed a landscape-scale numerical model that incorporates a spatially variable suspended sediment concentration and calculates biomass for multiple plant species across the marsh platform. The model domain comprised all areas of PIE (excluding ponds) within the elevation range:

$$-\left(\frac{\delta z}{2}\right) \leq Z(x,y,t) \leq Z_{max} + MSL \quad (1)$$

where $Z(x,y,t)$ is the elevation (relative to MSL) of a location (x, y) at time t, δz is the tidal range, and Z_{max} is defined as $\delta z^2/4$. The domain included the entire elevational extent of marshes at PIE, as well as areas of water and uplands within the elevation range. Elevations of water and uplands

within the domain were updated each time step relative to MSL. Marsh replaced water and uplands when elevations were within marsh range. Accretion was only calculated in marsh. The change in elevation in response to mineral and organic accretion (with rates A_m and A_o, respectively) under a relative SLR of rate R, is given by the mass balance:

$$\frac{\partial Z}{\partial t} = A_m(x, y, Z) + A_o(x, y, Z) - R \quad (2)$$

where A_m is a function of elevation and distance from the nearest channel or mudflat, and A_o is a function of elevation (Fig. 2). For simplicity, we assume no net mineral accretion within intertidal open waters, including ponds, and passive inundation of upland areas ($\partial Z/\partial t = -R$).

Mineral accretion model

We employed a simplified 1D transport model (Vinent et al. 2019), in which the decrease of mineral accretion rates (A_m) with distance l to the nearest channel/mudflat (Fig. 2a) can be approximated by an exponential function:

$$A_m(x, y, Z) = A_m^{max}(Z)\, e^{-\frac{l(x,y)}{L_c}} \quad (3)$$

where A_m^{max} is a reference accretion rate, and L_c is a length characterizing the spatial decay of mineral accretion. From mass conservation, the reference accretion rate A_m^{max} is proportional to the sediment concentration at the marsh edge (C_0), an effective falling velocity w_f and the rescaled local inundation time (average fraction of time below water) $\tau(Z) = \pi^{-1}\cos^{-1}(2Z/\delta z)$:

$$A_m^{max}(Z) = \frac{C_0 w_f}{\rho_m}\tau(Z)\, r\left(\frac{w_f T}{\delta z}\right) \quad (4)$$

where ρ_m is the density of mineral sediments deposited on the marsh, and the fitting function $r = \left(1 + \left(1 + w_f T/\delta z\right)^{-1}\right)/2$ (with values between 0.5 and 1) represents the effect of sediment inertia in the temporal decrease of suspended sediments during ebb flows.

171 The decay length L_c was found to scale with the ratio of tidal water discharge per unit
172 width and the effective falling velocity:

173 $$L_c = \beta \frac{L\delta z}{Tw_s} \quad (5)$$

174 where $L(x,y)$ is the length of the local drainage basin, T is the tidal period, w_s is the settling
175 velocity, and $\beta = 1.5$ is a fitting parameter. After calculating the distance $l(x,y)$ to the
176 channel/mudflat—defined by the MSL contour line ($Z(x,y) = 0$)—we relate each point (x,y) to
177 the closer local maximum of the distance to the channel field. We then define the drainage length
178 $L(x,y)$ associated with that point as the distance to the channel of that local maximum.

179 Organic accretion model

180 The organic accretion model incorporated biomass productivity for *S. alterniflora* and *S.*
181 *patens* to account for differing contributions of organic material in low and high marsh
182 environments. The rate of organic accretion (A_o) was determined by the following equation:

183 $$A_o(x,y,Z) = \frac{kB_iP_i}{\rho_o} \quad (6)$$

184 where *k* is the recalcitrant fraction coefficient, assumed to be the lignin content of belowground
185 biomass (Benner et al. 1984), B_i is the ratio of below- to aboveground biomass for plant species
186 *i*, P_i is the aboveground biomass for species *i*, and ρ_o is the density of organic sediments.
187 Aboveground biomass is a function of elevation, following the parabolic relationship described
188 by Morris (2002):

189 $$P_i(x,y,Z) = aZ + bZ^2 + c \quad (7)$$

190 where *a*, *b*, and *c* are coefficients that determine the upper and lower elevation limits of biomass
191 for species *i*. To compute biomass corresponding with elevation *Z* at location (*x,y*), coefficient
192 $a = P_i^{max}\left(Z_i^{min} + Z_i^{max}\right)/M$, in which P_i^{max} is the maximum aboveground biomass for species
193 *i*, Z_i^{min} and Z_i^{max} are minimum and maximum elevations at which aboveground biomass for

194 species *i* is calculated, and $M = \left[\left(Z_i^{max} - Z_i^{min}\right)/2\right]^2$. Coefficient $b = -P_i^{max}/M$, and $c =$

195 $\left(-P_i^{max} Z_i^{min} Z_i^{max}\right)/M$.

196 Biomass elevation ranges differed from elevation distributions of *S. alterniflora* and *S.*

197 *patens* because elevation distributions did not overlap in the model (i.e., only one plant species

198 occurred at a given elevation). The elevation marking the transition from low to high marsh

199 (described below under Model parameterization) did not correspond with upper and lower

200 elevation limits supporting biomass of *S. alterniflora* and *S. patens*, respectively. Rather,

201 biomass elevation limits for the two species overlapped (Fig. 2b).

202 *Model parameterization*

203 To parameterize the model, we used spatial data, existing field measurements, and

204 literature on PIE (Table 1). Initial elevations for the model (2011) were defined by a vegetation-

205 corrected digital elevation model (DEM) with a resolution of 1 m^2, derived from 2011 LiDAR

206 (referenced to NAVD 88; Edwards 2016). The DEM was converted to a spatial resolution of 10

207 m^2 before being applied to the model. The model converted the vertical datum to mean sea level

208 (MSL); unless otherwise stated, all reported elevations are relative to MSL. Initial land cover

209 was defined by a habitat raster for PIE based on the DEM and included four categories: water,

210 low marsh, high marsh, and upland (Edwards 2016). We used the DEM and habitat rasters to

211 create probability distributions of low and high marsh plants across elevation. We used these

212 distributions to assign the elevation limits for low and high marsh (0.109 m and 1.81 m,

213 respectively) and the transition elevation between low and high marsh (1.09 m), which

214 corresponded with elevations where the probability of *S. alterniflora* and *S. patens* occurrences

215 was approximately 50%. Since *S. alterniflora* can occur across the entire marsh elevation range,

216 the upper elevation limit for *S. alterniflora* biomass was the same as the high marsh upper

217 elevation limit (1.81 m). The lower elevation limit for *S. patens* biomass was 0.4 m. Biomass
218 elevation limits for both species were consistent with species elevation range limits previously
219 developed from ground-truthed spectral classifications and 2011 LiDAR (Edwards 2016).
220 Elevations for peak biomass occurred at the midpoints of the biomass elevation ranges.
221 Maximum aboveground biomass for each species was estimated from field data (Morris and
222 Sundberg 2013a; b; Morris et al. 2013). Because reported ratios in the region vary widely
223 (Valiela et al. 1976; Deegan et al. 2012), below- to aboveground ratios for *S. alterniflora* (4.5)
224 and *S. patens* (1.8) were assigned that produced modeled accretion rates similar to observed
225 rates.

226 *Model validation*

227 We compared modeled initial accretion rates (t=1) under the historical rate of SLR (2.83
228 mm y^{-1}) to observed rates of elevation change from 11 surface elevation tables (SETs) installed
229 at PIE, as well as observed accretion rates from 1 SET and 3 ^{210}Pb cores for which elevation
230 change rates were not available (Wilson et al. 2014). Because the model treats accretion and
231 elevation change in the marsh as synonymous, we included both types of observed data in our
232 comparison. Modeled initial accretion rates closely matched observed data (Fig. 3; paired t = -
233 0.295, df=14, p = 0.799). More than half (60%) of modeled rates were within 1 mm of observed
234 rates and all but 2 were within 2 mm. Mean modeled accretion rate among low marsh sites (n=6)
235 was 6.29 mm y^{-1} compared to a mean observed rate of 6.77 mm y^{-1}. Mean modeled accretion rate
236 at high marsh sites (n=9) was 2.91 mm y^{-1} compared to a mean observed rate of 2.73 mm y^{-1}.

237 *Model sensitivity and uncertainty*

238 To determine the sensitivity of modeled output to mineral and organic accretion
239 variables, we conducted a global sensitivity analysis using the Morris method (Morris 1991). We

240 tested model sensitivity to 8 variables we expected to have the most influence on modeled
241 accretion rates: C_0, w_s, P_i, B_i, k, and DEM elevation error (E_{DEM}). The DEM elevation error was
242 included to account for potential discrepancies between the DEM and actual ground elevations.
243 We computed the mean elementary effect of each variable using UQLab v1.3 for Matlab based
244 on 20 combinations of input variable values randomly generated from uniform distributions
245 (requiring 180 model runs). Mean elementary effects (EE) indicated that accretion rates were
246 robust to input variables. Among mineral accretion parameters, C_0 had more influence than w_s
247 (mean EE = 0.09). Among organic accretion parameters, P_{SP} and k had the most influence (mean
248 EE of 0.34 and 0.50, respectively) and the strongest interaction effects among all variables.
249 Biomass ratios had no influence, and P_{SA} had negligible influence (mean EE = 0.02). The
250 influence of E_{DEM} was similar to P_{SP} (mean EE = 0.32).
251 We incorporated uncertainty into our model experiments to account for natural variation
252 and uncertainty of input parameters, informed by the sensitivity analysis. Model experiments
253 (described below) included a range of input values for C_0, P_{SA}, P_{SP}, and E_{DEM}. Because the
254 sensitivity analysis indicated interaction effects between P_{SP} and k, we included variation for P_{SA}
255 and P_{SP} to represent uncertainty in organic accretion. Values were randomly generated from
256 uniform distributions; bounds for distributions were determined using literature and PIE field
257 data (Table 1).
258 *Model experiments*
259 To evaluate the vulnerability of PIE marshes to SLR, we simulated accretion rates on an
260 annual time step for 90 years (2011-2100) under three scenarios of projected SLR (historical,
261 medium, high). Rates of SLR were based on three emissions scenarios described in the IPCC
262 Fifth Assessment Report (IPCC 2013): historical (2.83 mm y^{-1}), RCP 6.0 (medium; 8.72 mm y^{-1}

263 by 2100), and RCP 8.5 (high; 18.5 mm y^{-1} by 2100), and were adjusted for local subsidence
264 inferred from Boston, MA (1921-2018). We determined marsh vulnerability by examining
265 accretion rates, relative elevations, landscape composition, and areal extent of PIE marshes over
266 time and comparing results for 2100 to initial conditions in 2011. Results are reported as
267 means±1 SD computed from 300 model runs of each SLR scenario.

268 To test whether reducing human impacts increased the threshold rate of SLR that PIE
269 marshes could survive, we compared maximum mineral accretion rates across the marsh
270 landscape using a suspended sediment concentration of 15 mg L^{-1}, and a hypothetical increased
271 suspended sediment concentration of 30 mg L^{-1}. Maximum accretion rates were calculated by
272 setting the elevation of every point on the marsh to the minimum low marsh elevation (i.e., the
273 minimum elevation at which *S. alterniflora* grows and the elevation at which maximum mineral
274 accretion occurs in the marsh). For this test, all input variables were fixed. We used the midpoint
275 values (1000 g m^{-2} and 1250 g m^{-2}) from the uncertainty ranges for maximum aboveground
276 biomass for *S. alterniflora* and *S. patens,* respectively. We evaluated the distribution of mineral
277 deposition across the marsh landscape by comparing mineral accretion rates near tidal channels
278 and in the marsh interior under both suspended sediment concentration scenarios. The distance
279 defining marsh edge and marsh interior was based on a sediment transport length of 43.5 m
280 (Zhang et al. 2019).

281 Results

282 *Vertical accretion*

283 The numerical model predicted high initial vertical accretion rates across PIE marshes
284 relative to the historical rate of SLR. The mean initial vertical accretion rate from 300 model
285 runs was 3.45±0.83 mm y^{-1}, with higher rates reaching 9.28±1.11 mm y^{-1} at lower elevations and

near channels. Accretion rates were dominated by organic accretion, which averaged 2.59 ±0.51 mm y^{-1} and represented 75% of total accretion. The mean organic accretion rate was twice as fast in low marsh (4.47±0.57 mm y^{-1}) compared to high marsh (2.19±0.38 mm y^{-1}), while the rate of mineral accretion, which averaged 0.86±0.37 mm y^{-1}, was 5 times faster in low marsh (2.63±0.55 mm y^{-1}) compared to high marsh (0.52±0.28 mm y^{-1}). Maximum mineral accretion occurred near channels, reaching 7.59±1.49 mm y^{-1}.

Under the historical SLR scenario (2.83 mm y^{-1}), vertical accretion rates equilibrated toward the rate of SLR over time to 3.04±0.39 mm y^{-1} (Fig. 4a). Under higher SLR scenarios, accretion rates increased through time (5.54 ±0.81 and 7.02±0.71 mm y^{-1} in 2100 for medium and high SLR scenarios, respectively), but were slower than SLR rates, which resulted in declining marsh elevations (Fig. 4b). Under the medium SLR scenario (8.72 mm y^{-1} by 2100), most of the marsh area was in an accretion deficit relative to the rate of SLR by 2100. Only in low marsh along tidal channels and the Rowley River did accretion rates exceed the rate of SLR (reaching 9.27±1.13 mm y^{-1}; Fig. 5). An accretion deficit occurred at every position on the marsh by 2100 under a high rate of SLR (18.5 mm y^{-1} by 2100). Accretion was fastest in low marsh along tidal channels and the Rowley River. The maximum accretion rate (9.33±1.10 mm y^{-1}) in 2100 was approximately half the rate of SLR.

Elevation and MSL

In 2011, modeled mean marsh elevation (excluding ponds) was 1.27±0.10 m above MSL (Fig. 4b). Under the historical rate of SLR, MSL increased 0.25 m by 2100 while mean marsh elevation increased to 1.31±0.06 m above MSL. The distribution of marsh elevations in 2100 largely overlapped with elevations in 2011, but the frequency of higher elevations increased, resulting in more high marsh (Fig. 6, Table 2). Mean sea level increased 0.60 m under the

309 medium SLR scenario and marsh elevation decreased to 1.09±0.04 m (Fig. 4b). Mean elevation
310 occurred at the transition elevation from low to high marsh, resulting in increased frequencies of
311 elevations within the low marsh range and near the lower elevation limit of high marsh by 2100
312 (Fig. 6). Under the high SLR scenario, MSL increased 1.02 m and mean marsh elevation
313 dropped below the high marsh elevation range to 0.81±0.05 m (Fig. 4b). Little overlap remained
314 between 2011 and 2100 elevation distributions as elevations across the marsh shifted into the low
315 marsh range (Fig. 6).
316 *Marsh habitat*
317 In 2011, high marsh occupied 33.4±3.33 km^2 and accounted for approximately 82% of
318 total marsh area (Table 2). Under the historical rate of SLR, high marsh occupied nearly all
319 (94%) of the total marsh area by 2100 as portions of adjacent uplands (1.7±0.19 km^2) and low
320 marsh (4.9±2.51 km^2) converted to high marsh (Fig. 7). Under a medium SLR scenario, high
321 marsh decreased in area (17.2±9.50 km^2), and no longer dominated the landscape in 2100
322 (occupying 39% of total marsh area). Mean low marsh area more than tripled (26.4±9.65 km^2),
323 due to the conversion of 20.3±7.0 km^2 of high marsh to low marsh. Because mean marsh
324 elevation in 2100 occurred at the transition from low to high marsh, even small differences in
325 elevation between model runs created large variation in low and high marsh extents. Total marsh
326 area increased to 43.6±0.28 km^2 as uplands (2.39±0.26 km^2) converted to high marsh and low
327 marsh (0.24±0.13 km^2) converted to open water. Under the high SLR scenario, PIE converted to
328 a low marsh-dominated system by 2060 (Fig. 8). By 2100, all high marsh present in 2011
329 converted to low marsh. The conversion of uplands to marsh (3.7±0.25 km^2) accounted for all
330 high marsh present in 2100 (8% of total marsh area). Approximately 1.19±0.28 km^2 of low
331 marsh converted to open water, largely in low marsh areas along the Rowley River. Despite

large-scale replacement of high marsh by low marsh, areal extent of PIE marshes increased to 44.2±0.28 km^2.

Dam removal

Supposing dam removal doubled suspended sediment concentration, the maximum mineral accretion rate would also approximately double near tidal channels and in the marsh interior. Near tidal channels, maximum accretion would increase by 5.96±1.33 mm y^{-1} (spatial mean) and by as much as 7.80 mm y^{-1}. In the marsh interior, the mean maximum accretion rate would increase by 4.10±0.96 mm y^{-1}, and by as much as 6.80 mm y^{-1} (Fig. 9).

Discussion

Model assumptions and advances

We created a model that incorporates spatially-variable nonlinear feedbacks characteristic of process-based models into a relatively simple, easily parameterized numerical model. Within the marsh, elevation change depended entirely on accretion rates because shallow subsidence at Plum Island is negligible (Hopkinson et al. 2018). Ponds were treated as static features and excluded from the model domain; though pond formation is cyclical, their extent is stable on the time-scale simulated in our model. Consistent with other landscape models, we excluded erosion as a driver of marsh area loss. Though an important source of internal sediment, marsh edge erosion throughout the entire estuary currently accounts for <0.1% of total marsh area per year (Hopkinson et al. 2018). To maintain simplicity, the model also excluded processes that are not direct results of SLR, including nutrient-induced channel widening, sediment displacement and accumulation from ice rafting, and factors beyond SLR-driven geomorphic feedbacks that contribute to pond formation (Deegan et al. 2012; Wilson et al. 2014). The focus was to advance landscape models by including dynamic, spatially variable mineral accretion rates that explicitly

relate marsh vulnerability to sediment availability across the marsh platform, and organic accretion rates for multiple plant species that reflect rates specific to low and high marsh zones. Therefore, at a given elevation in a marsh landscape, the model accounts for the range of accretion rates that occur with respect to elevation, distance from the nearest channel, and local drainage basin size (Fig. 2). The close approximation of modeled accretion rates to long-term observed rates of elevation change and accretion spanning low and high marsh zones demonstrates the proficiency of the model in capturing on-the-ground vertical change (Fig. 3).

Long-term responses of PIE marshes to SLR

Model results suggest that PIE marshes will keep pace with the historical rate of SLR (2.83 mm y^{-1}) through 2100, despite low sediment supply, high tidal range, and limited opportunity for lateral retreat (Fig. 4, 5a). The initial mean accretion rate (3.45±0.83 mm y^{-1}) exceeds the historical rate of SLR, implying that combined mineral and organic sediments are sufficient to maintain elevation relative to MSL and preserve areal extents of low and high marsh. Accretion is expected to decrease towards the rate of SLR over time, signaling that PIE marshes are in a state of dynamic equilibrium. This model prediction is consistent with other research on PIE marshes. Previous numerical modeling of a generic marsh with conditions similar to Plum Island suggested that PIE marshes could persist in meta-equilibrium under the current rate of SLR despite having reduced sediment supply (Kirwan et al. 2011). Analysis of historical imagery, sediment cores, and field experimentation likewise revealed the marshes are in dynamic equilibrium, evidenced by the cyclical dynamics of pond formation and recovery across the marsh platform (Wilson et al. 2014). Observed rates of elevation change and accretion that currently enable PIE marshes to maintain equilibrium are comparable to initial modeled accretion rates generated under the historical rate of SLR (Wilson et al. 2014).

Model results, however, strongly suggest current sediment supply will be inadequate under medium and high rates of SLR (Fig. 4a, 5b, 5c). While marsh areal extent remained stable, slower accretion rates relative to medium and high rates of SLR drove elevation decline relative to sea level (Fig. 4b, 6). In response, flood-tolerant *S. alterniflora* supplanted *S. patens* in areas where elevation decreased below the range limit for *S. patens* (Fig. 7b, 8, Table 2). *Spartina patens*, which cannot tolerate anoxic soils typical of low marsh (Bertness 1991), was completely replaced by *S. alterniflora* under a high rate of SLR as PIE converted to a low marsh system. Plant productivity experiments at PIE have also indicated accelerated rates of SLR would lead to eventual loss of *S. patens* (Morris et al. 2013). Predicted conversion to low marsh at PIE is consistent with vegetation responses already underway in other New England marshes experiencing elevation declines relative to sea level (Watson et al. 2016). As the rate of SLR has outpaced accretion rates at Headquarters Marsh in Little Narragansett Bay, CT, *S. alterniflora* and other low marsh plants have replaced *S. patens* over the past 50+ years (Warren and Niering 1993). In Narragansett Bay, RI, SLR-induced migration of *S. alterniflora* into high marsh has been underway for at least 20 years (Donnelly and Bertness 2001). In regions where landward migration is possible, new high marsh supporting *S. patens* can develop in adjacent uplands. At PIE and other systems where room for migration is severely restricted, low marsh conversion will be coupled with loss of *S. patens* and its attendant ecological functions, namely, fixing nitrogen via mycorrhizae and providing habitat for nesting birds (Watson et al. 2016).

Accelerated accretion rates tend to accompany high to low marsh conversion as increased sediment delivery and contingent plant productivity accompany increased flooding. At PIE, accretion rates at low marsh SET and core sites are approximately 2.5 times higher than high marsh sites (Wilson et al. 2014). Model results predicted accretion rates would increase 61% and

401 103% by 2100 under medium and high rates of SLR, respectively, as the extent of low marsh
402 increases (Fig. 4). Typically, the feedback between accretion rates and MSL enables low marsh
403 elevations to stabilize relative to SLR (Kirwan et al. 2016a). For example, increased inundation
404 led to increased mineral deposition on undisturbed marshes in Long Island, NY, driving higher
405 accretion rates and promoting marsh resilience (Kolker et al. 2010). When elevation decreases
406 within the range supporting peak productivity of low marsh plants, organic accretion and
407 increased carbon storage also enable marsh elevation to stabilize relative to sea level, as
408 demonstrated in New England marshes in Cape Cod, MA (Gonneea et al. 2019). However,
409 similar to other sediment-poor, organic-rich New England marshes (Carey et al. 2017), our
410 model predictions suggest reduced sediment availability at PIE will prevent marsh elevation
411 from stabilizing even as accretion rates increase across an expanding low marsh. Even if the
412 maximum accretion rate predicted in 2100 (9.33±1.10 mm y^{-1}) occurred at every position of the
413 marsh platform, it would be insufficient to stabilize the elevation under a high rate of SLR.
414 Human impacts increase marsh vulnerability to SLR by disrupting feedbacks that drive
415 vertical accretion and restricting lateral migration (Kennish 2001; Kirwan and Megonigal 2013).
416 Plum Island marshes are restricted primarily by sediment availability, which is naturally low in
417 the region, and has been reduced further by human activities. Dams on the rivers feeding into
418 PIE as well as extensive freshwater marsh and forest upstream limit sediment delivery to <10%
419 of what is required for the marsh platform to maintain its elevation relative to sea level
420 (Hopkinson et al. 2018). Consequently, marshes must depend on marsh edge erosion, the ocean,
421 and/or tidal flat erosion as primary sediment sources. Edge erosion potentially provides 31% of
422 sediment needed to maintain marsh elevation under the current rate of SLR; sediment mass
423 balance by Hopkinson et al. 2018 implies that the ocean and tidal flat erosion provide the

424 remaining sediment required for marsh accretion. Whether these sources can provide sufficient
425 sediment under accelerated rates of SLR may largely dictate long-term marsh survival.
426 We considered a hypothetical case in which removing the dam on the Ipswich River
427 located at the head of tide doubled suspended sediment concentration to 30 mg L^{-1} (Fig. 9).
428 Removal of this dam is an action under consideration by local officials that could increase
429 sediment loading and prolong salt marsh survival (Hopkinson et al. 2018). Such increases could
430 potentially enable mean vertical accretion to equilibrate to a medium rate of SLR (predicted to be
431 5.54±0.81 mm y^{-1} by 2100 under the current suspended sediment concentration) and reduce
432 marsh conversion under a high rate of SLR. Nevertheless, these are simplistic predictions
433 because we have not modeled how dam removal would actually change suspended sediment
434 concentrations.
435 *PIE vulnerability vs. elevation capital*
436 Salt marsh vulnerability to SLR is generally thought to depend on sediment availability,
437 tidal range, and opportunity for landward migration. Marshes with insufficient sediment supply
438 or unavailable surrounding uplands are frequently reported to be more susceptible to drowning
439 than marshes with adequate sediment and accessible uplands (Reed 1995; FitzGerald et al. 2008;
440 Kirwan et al. 2010; Day et al. 2011; Doody 2013). For example, sediment-deficient coastal
441 wetlands along the East and Gulf Coasts of the US fed by dammed rivers and subject to higher
442 rates of SLR are particularly vulnerable to drowning (Weston 2014). Previous numerical
443 modeling has emphasized vertical and lateral constraints on wetland adaptability. Tidal marshes
444 lacking available adjacent uplands in the San Francisco Bay Estuary were identified as less
445 resilient to accelerated rates of SLR than marshes with room to migrate landward according to
446 results from a MEM model (Schile et al. 2014). Likewise, marshes with low vertical accretion

447 and limited opportunity for migration along the US Pacific Coast face a high risk of drowning by
448 2110 based on WARMER model results (Thorne et al. 2018). Results of a Hydro-MEM model
449 also demonstrated that the portions of marshes in Florida most susceptible to drowning under
450 accelerated rates of SLR were in areas with limited room for migration (Alizad et al. 2016a; b).
451 In contrast to previous work linking marsh vulnerability to sediment supply and landward
452 migration, we found that PIE marshes are not immediately vulnerable to drowning despite their
453 low sediment supply and migration potential. The areal extent of PIE was preserved even as
454 accretion rates failed to keep pace and marsh elevation decreased because marshes in the estuary
455 have high elevation capital. Elevation capital, or the vertical accumulation of material during
456 marsh development that contributes to marsh elevation, provides marshes with a vertical reserve
457 even when accretion rates cannot keep pace with SLR (Reed 2002; Cahoon and Guntenspergen
458 2010).
459 The finding that elevation capital prolongs marsh survival is consistent with previous
460 work. For example, Cahoon et al. (2019) found that among marshes with the same sediment
461 source and subject to the same tidal range and rate of SLR in Jamaica Bay, NY, those with high
462 elevation capital maintained their relative elevation, while the low elevation marsh depleted its
463 vertical reserve and deteriorated. Marshes with elevation capital in southern New England were
464 also found to be more stable because they produced more belowground biomass than lower,
465 more frequently inundated marshes experiencing decline (Watson et al. 2017). However,
466 elevation capital does not always alleviate the risk of drowning. Marshes along the US Pacific
467 Coast were predicted to be highly susceptible to submergence due to low sediment supply and
468 restricted lateral movement, despite having high elevation capital (Thorne et al. 2018).

For PIE marshes, high elevation capital does not eliminate the long-term threat of marsh loss under accelerated SLR but slows the rate at which loss occurs. Our model predicts widespread vegetation change, accretion deficits across the marsh, including in low marsh areas near channels where mineral accretion is highest, and trajectories of decreasing elevation under medium and high rates of SLR. Therefore, PIE marshes could eventually be vulnerable to drowning, but on a timeline that extends beyond 2100. Although sediment-deficient marshes with limited migration space are considered extremely vulnerable to SLR (Reed 1995; Kirwan et al. 2016b; Raposa et al. 2017; Thorne et al. 2018), our results highlight that marshes with high elevation capital can maintain their areal extent for decades to centuries even under conditions in which they will inevitably drown.

480 References

481 Alizad, K., S. C. Hagen, J. T. Morris, P. Bacopoulos, M. V. Bilskie, J. F. Weishampel, and S. C.
482 Medeiros. 2016a. A coupled, two-dimensional hydrodynamic-marsh model with biological
483 feedback. Ecol. Modell. 327: 29–43, doi:10.1016/j.ecolmodel.2016.01.013

484 Alizad, K., S. C. Hagen, J. T. Morris, S. C. Medeiros, M. V. Bilskie, and J. F. Weishampel.
485 2016b. Coastal wetland response to sea-level rise in a fluvial estuarine system. Earth's
486 Futur. 4: 483–497, doi:10.1002/2016EF000385

487 Bamber, J. L., M. Oppenheimer, R. E. Kopp, W. P. Aspinall, and R. M. Cooke. 2019. Ice sheet
488 contributions to future sea-level rise from structured expert judgment. Proc. Natl. Acad. Sci.
489 USA 116: 11195–11200, doi:10.1073/pnas.1817205116

490 Benner, R., S. Y. Newell, A. E. Maccubbin, and R. E. Hodson. 1984. Relative contributions of
491 bacteria and fungi to rates of degradation of lignocellulosic detritus in salt-marsh sediments.
492 Appl. Environ. Microbiol. 48: 36–40.

493 Bertness, M. D. 1991. Zonation of *Spartina patens* and *Spartina alterniflora* in New England salt
494 marsh. Ecology 72: 138–148, doi:10.2307/1938909

495 Borchert, S. M., M. J. Osland, N. M. Enwright, and K. T. Griffith. 2018. Coastal wetland
496 adaptation to sea level rise: Quantifying potential for landward migration and coastal
497 squeeze. J. Appl. Ecol. 55: 2876–2887, doi:10.1111/1365-2664.13169

498 Cadol, D., A. J. Elmore, S. M. Guinn, K. A. M. Engelhardt, and G. Sanders. 2016. Modeled
499 tradeoffs between developed land protection and tidal habitat maintenance during rising sea
500 levels. PLoS One 11: e0164875, doi:10.1371/journal.pone.0164875

501 Cadol, D., K. Engelhardt, A. Elmore, and G. Sanders. 2014. Elevation-dependent surface
502 elevation gain in a tidal freshwater marsh and implications for marsh persistence. Limnol.

503 Oceanogr. 59: 1065–1080, doi:10.4319/lo.2014.59.3.1065
504 Cahoon, D. R., and G. R. Guntenspergen. 2010. Climate change, sea-level rise, and coastal
505 wetlands. Natl. Wetl. Newsl. 32: 8–12.
506 Cahoon, D. R., J. C. Lynch, C. T. Roman, J. P. Schmit, and D. E. Skidds. 2019. Evaluating the
507 relationship among wetland vertical development, elevation capital, sea-level rise, and tidal
508 marsh sustainability. Estuar. Coasts 42: 1–15, doi:10.1007/s12237-018-0448-x
509 Carey, J. C., S. B. Moran, R. P. Kelly, A. S. Kolker, and R. W. Fulweiler. 2017. The declining
510 role of organic matter in New England salt marshes. Estuar. Coasts 40: 626–639,
511 doi:10.1007/s12237-015-9971-1
512 Carniello, L., A. Defina, and L. D'Alpaos. 2009. Morphological evolution of the Venice lagoon:
513 Evidence from the past and trend for the future. J. Geophys. Res. 114: F04002,
514 doi:10.1029/2008JF001157
515 Crosby, S. C., D. F. Sax, M. E. Palmer, H. S. Booth, L. A. Deegan, M. D. Bertness, and H. M.
516 Leslie. 2016. Salt marsh persistence is threatened by predicted sea-level rise. Estuarine,
517 Coastal Shelf Sci. 181: 93–99, doi:10.1016/J.ECSS.2016.08.018
518 D'Alpaos, A., S. Lanzoni, M. Marani, and A. Rinaldo. 2007. Landscape evolution in tidal
519 embayments: Modeling the interplay of erosion, sedimentation, and vegetation dynamics. J.
520 Geophys. Res. 112: F01008, doi:10.1029/2006JF000537
521 Day, J. W., G. P. Kemp, D. J. Reed, D. R. Cahoon, R. M. Boumans, J. M. Suhayda, and R.
522 Gambrell. 2011. Vegetation death and rapid loss of surface elevation in two contrasting
523 Mississippi delta salt marshes: The role of sedimentation, autocompaction and sea-level
524 rise. Ecol. Eng. 37: 229–240, doi:10.1016/j.ecoleng.2010.11.021
525 Deegan, L. A., D. S. Johnson, R. S. Warren, B. J. Peterson, J. W. Fleeger, S. Fagherazzi, and W.

526 M. Wollheim. 2012. Coastal eutrophication as a driver of salt marsh loss. Nature 490: 388–
527 392, doi:10.1038/nature11533
528 Donnelly, J. P., and M. D. Bertness. 2001. Rapid shoreward encroachment of salt marsh
529 cordgrass in response to accelerated sea-level rise. Proc. Natl. Acad. Sci. USA 98: 14218–
530 14223, doi:10.1073/pnas.251209298
531 Doody, J. P. 2013. Coastal squeeze and managed realignment in southeast England, does it tell
532 us anything about the future? Ocean Coast. Manag. 79: 34–41,
533 doi:10.1016/j.ocecoaman.2012.05.008
534 Edwards, J. D. 2016. Applicability of LiDAR technology in saltmarshes : Landscape-scale
535 predictive models to local-scale biomass estimation. Master's thesis. University of South
536 Carolina.
537 Enwright, N. M., K. T. Griffith, and M. J. Osland. 2016. Barriers to and opportunities for
538 landward migration of coastal wetlands with sea-level rise. Front. Ecol. Environ. 14: 307–
539 316, doi:10.1002/fee.1282
540 Fagherazzi, S. and others. 2012. Numerical models of salt marsh evolution: Ecological,
541 geomorphic, and climatic factors. Rev. Geophys. 50: RG1002, doi:10.1029/2011RG000359
542 FitzGerald, D. M., M. S. Fenster, B. A. Argow, and I. V. Buynevich. 2008. Coastal impacts due
543 to sea-level rise. Annu. Rev. Earth Planet. Sci. 36: 601–647,
544 doi:10.1146/annurev.earth.35.031306.140139
545 FitzGerald, D. M., and Z. Hughes. 2019. Marsh processes and their response to climate change
546 and sea-level rise. Annu. Rev. Earth Planet. Sci. 47: 481–517, doi:10.1146/annurev-earth-
547 082517-010255
548 French, J. 2006. Tidal marsh sedimentation and resilience to environmental change: Exploratory

549 modelling of tidal, sea-level and sediment supply forcing in predominantly allochthonous
550 systems. Mar. Geol. 235: 119–136, doi:10.1016/j.margeo.2006.10.009
551 Friedrichs, C. T., and J. E. Perry. 2001. Tidal salt marsh morphodynamics: A synthesis. J.
552 Coastal Res. 27: 7–37.
553 Gittman, R. K., F. J. Fodrie, A. M. Popowich, D. A. Keller, J. F. Bruno, C. A. Currin, C. H.
554 Peterson, and M. F. Piehler. 2015. Engineering away our natural defenses: An analysis of
555 shoreline hardening in the US. Front. Ecol. Environ. 13: 301–307, doi:10.1890/150065
556 Gleason, M. L., D. A. Elmer, N. C. Pien, and J. S. Fisher. 1979. Effects of stem density upon
557 sediment retention by salt marsh cord grass, *Spartina alterniflora* Loisel. Estuaries 2: 271–
558 273, doi:10.2307/1351574
559 Gonneea, M. E. and others. 2019. Salt marsh ecosystem restructuring enhances elevation
560 resilience and carbon storage during accelerating relative sea-level rise. Estuarine, Coastal
561 Shelf Sci. 217: 56–68, doi:10.1016/j.ecss.2018.11.003
562 Gu, J., M. Luo, X. Zhang, G. Christakos, S. Agusti, C. M. Duarte, and J. Wu. 2018. Losses of
563 salt marsh in China: Trends, threats and management. Estuarine, Coastal Shelf Sci. 214: 98–
564 109, doi:10.1016/j.ecss.2018.09.015
565 Hopkinson, C. S., J. T. Morris, S. Fagherazzi, W. M. Wollheim, and P. A. Raymond. 2018.
566 Lateral marsh edge erosion as a source of sediments for vertical marsh accretion. J.
567 Geophys. Res. Biogeosci. 123: 2444–2465, doi:10.1029/2017JG004358
568 Horton, B. P., S. Rahmstorf, S. E. Engelhart, and A. C. Kemp. 2014. Expert assessment of sea-
569 level rise by AD 2100 and AD 2300. Quat. Sci. Rev. 84: 1–6,
570 doi:10.1016/j.quascirev.2013.11.002
571 IPCC. 2013. Climate Change 2013: The Physical Science Basis. Contribution of Working Group

572 I to the Fifth Assessment Report of the Intergovernmental Panel on Climate Change In T.F.
573 Stocker et al. [eds.].doi:10.1017/CBO9781107415324
574 Jankowski, K. L., T. E. Törnqvist, and A. M. Fernandes. 2017. Vulnerability of Louisiana's
575 coastal wetlands to present-day rates of relative sea-level rise. Nat. Commun. 8: 14792,
576 doi:10.1038/ncomms14792
577 Kearney, M. S., A. S. Rogers, J. R. G. Townshend, E. Rizzo, D. Stutzer, J. C. Stevenson, and K.
578 Sundborg. 2002. Landsat imagery shows decline of coastal marshes in Chesapeake and
579 Delaware Bays. Eos, Trans. Am. Geophys. Union 83: 173–178,
580 doi:10.1029/2002EO000112
581 Kennish, M. J. 2001. Coastal salt marsh systems in the U.S.: A review of anthropogenic impacts.
582 J. Coastal Res. 17: 731–748.
583 Kirwan, M. L., and K. B. Gedan. 2019. Sea-level driven land conversion and the formation of
584 ghost forests. Nat. Clim. Change 9: 450–457, doi:10.1038/s41558-019-0488-7
585 Kirwan, M. L., and G. R. Guntenspergen. 2012. Feedbacks between inundation, root production,
586 and shoot growth in a rapidly submerging brackish marsh. J. Ecol. 100: 764–770,
587 doi:10.1111/j.1365-2745.2012.01957.x
588 Kirwan, M. L., G. R. Guntenspergen, A. D'Alpaos, J. T. Morris, S. M. Mudd, and S.
589 Temmerman. 2010. Limits on the adaptability of coastal marshes to rising sea level.
590 Geophys. Res. Lett. 37: L23401, doi:10.1029/2010GL045489
591 Kirwan, M. L., and J. P. Megonigal. 2013. Tidal wetland stability in the face of human impacts
592 and sea-level rise. Nature 504: 53–60.
593 Kirwan, M. L., and A. B. Murray. 2007. A coupled geomorphic and ecological model of tidal
594 marsh evolution. Proc. Natl. Acad. Sci. USA 104: 6118–6122,

595 doi:10.1073/pnas.0700958104
596 Kirwan, M. L., A. B. Murray, J. P. Donnelly, and D. R. Corbett. 2011. Rapid wetland expansion
597 during European settlement and its implication for marsh survival under modern sediment
598 delivery rates. Geology 39: 507–510, doi:10.1130/G31789.1
599 Kirwan, M. L., S. Temmerman, E. E. Skeehan, G. R. Guntenspergen, and S. Fagherazzi. 2016a.
600 Overestimation of marsh vulnerability to sea level rise. Nat. Clim. Change 6: 253–260,
601 doi:10.1038/nclimate2909
602 Kirwan, M. L., D. C. Walters, W. G. Reay, and J. A. Carr. 2016b. Sea level driven marsh
603 expansion in a coupled model of marsh erosion and migration. Geophys. Res. Lett. 43:
604 4366–4373, doi:10.1002/2016GL068507
605 Kolker, A. S., M. L. Kirwan, S. L. Goodbred, and J. K. Cochran. 2010. Global climate changes
606 recorded in coastal wetland sediments: Empirical observations linked to theoretical
607 predictions. Geophys. Res. Lett. 37: L14706, doi:10.1029/2010GL043874
608 Langston, A. K., D. A. Kaplan, and F. E. Putz. 2017. A casualty of climate change? Loss of
609 freshwater forest islands on Florida's Gulf Coast. Glob. Chang. Biol. 23: 5383–5397,
610 doi:10.1111/gcb.13805
611 Li, H., and S. L. Yang. 2009. Trapping effect of tidal marsh vegetation on suspended sediment,
612 Yangtze Delta. J. Coastal Res. 254: 915–924, doi:10.2112/08-1010.1
613 Morris, J., and K. Sundberg. 2013a. Aboveground biomass data from control sites in a *Spartina*
614 *alterniflora*-dominated salt marsh at Law's Point, Rowley River, Plum Island Ecosystem
615 LTER, MA. Environ. Data Initiat., doi:10.6073/pasta/f089bf982920061722a03ec3f73b55e7
616 Morris, J., and K. Sundberg. 2013b. Aboveground biomass from control plots in a *Spartina*
617 *patens*-dominated salt marsh at Law's Point, Rowley River, Plum Island Ecosystem LTER,

618 MA. Environ. Data Initiat., doi:10.6073/pasta/2f253e2853b65c8e096f9b77099717a0
619 Morris, J. T. and others. 2016. Contributions of organic and inorganic matter to sediment volume
620 and accretion in tidal wetlands at steady state. Earth's Futur. 4: 110–121,
621 doi:10.1002/2015EF000334
622 Morris, J. T., P. V. Sundareshwar, C. T. Nietch, B. Kjerfve, and D. R. Cahoon. 2002. Responses
623 of coastal wetlands to rising sea level. Ecology 83: 2869–2877, doi:10.1890/0012-
624 9658(2002)083[2869:ROCWTR]2.0.CO;2
625 Morris, J. T., K. Sundberg, and C. S. Hopkinson. 2013. Salt marsh primary production and its
626 responses to relative sea level and nutrients in estuaries at Plum Island, Massachusetts, and
627 North Inlet, South Carolina, USA. Oceanography 26: 78–84, doi:10.2307/24862067
628 Morris, M. D. 1991. Factorial sampling plans for preliminary computational experiments.
629 Technometrics 33: 161–174, doi:10.1080/00401706.1991.10484804
630 Mudd, S. M., S. M. Howell, and J. T. Morris. 2009. Impact of dynamic feedbacks between
631 sedimentation, sea-level rise, and biomass production on near-surface marsh stratigraphy
632 and carbon accumulation. Estuarine, Coastal Shelf Sci. 82: 377–389,
633 doi:10.1016/j.ecss.2009.01.028
634 Murray, N. J., R. S. Clemens, S. R. Phinn, H. P. Possingham, and R. A. Fuller. 2014. Tracking
635 the rapid loss of tidal wetlands in the Yellow Sea. Front. Ecol. Environ. 12: 267–272,
636 doi:10.1890/130260
637 Nerem, R. S., B. D. Beckley, J. T. Fasullo, B. D. Hamlington, D. Masters, and G. T. Mitchum.
638 2018. Climate-change-driven accelerated sea-level rise detected in the altimeter era. Proc.
639 Natl. Acad. Sci. USA 115: 2022–2025, doi:10.1073/pnas.1717312115
640 Nyman, J. A., R. J. Walters, R. D. Delaune, and W. H. Patrick. 2006. Marsh vertical accretion

via vegetative growth. Estuarine, Coastal Shelf Sci. 69: 370–380, doi:10.1016/j.ecss.2006.05.041

Raposa, K. B., R. L. J. Weber, M. C. Ekberg, and W. Ferguson. 2017. Vegetation dynamics in Rhode Island salt marshes during a period of accelerating sea level rise and extreme sea level events. Estuar. Coasts 40: 640–650, doi:10.1007/s12237-015-0018-4

Redfield, A. C. 1972. Development of a New England salt marsh. Ecol. Monogr. 42: 201–237, doi:10.2307/1942263

Reed, D. J. 1995. The response of coastal marshes to sea-level rise: Survival or submergence? Earth Surf. Processes Landforms 20: 39–48, doi:10.1002/esp.3290200105

Reed, D. J. 2002. Sea-level rise and coastal marsh sustainability: Geological and ecological factors in the Mississippi delta plain. Geomorphology 48: 233–243, doi:10.1016/S0169-555X(02)00183-6

Rogers, K. and others. 2019. Wetland carbon storage controlled by millennial-scale variation in relative sea-level rise. Nature 567: 91–95, doi:10.1038/s41586-019-0951-7

Roner, M., A. D'Alpaos, M. Ghinassi, M. Marani, S. Silvestri, E. Franceschinis, and N. Realdon. 2016. Spatial variation of salt-marsh organic and inorganic deposition and organic carbon accumulation: Inferences from the Venice lagoon, Italy. Adv. Water Resour. 93: 276–287, doi:10.1016/J.ADVWATRES.2015.11.011

Schalles, J. F., C. M. Hladik, A. A. Lynes, and S. C. Pennings. 2013. Landscape estimates of habitat types, plant biomass, and invertebrate densities in a Georgia salt marsh. Oceanography 26: 88–97, doi:10.2307/24862069

Schieder, N. W., D. C. Walters, and M. L. Kirwan. 2018. Massive upland to wetland conversion compensated for historical marsh loss in Chesapeake Bay, USA. Estuar. Coasts 41: 940–

951, doi:10.1007/s12237-017-0336-9

Schile, L. M., J. C. Callaway, J. T. Morris, D. Stralberg, V. T. Parker, and M. Kelly. 2014. Modeling tidal marsh distribution with sea-level rise: Evaluating the role of vegetation, sediment, and upland habitat in marsh resiliency. PLoS One 9: e88760, doi:10.1371/journal.pone.0088760

Schuerch, M. and others. 2018. Future response of global coastal wetlands to sea-level rise. Nature 561: 231–234, doi:10.1038/s41586-018-0476-5

Swanson, K. M., J. Z. Drexler, D. H. Schoellhamer, K. M. Thorne, M. L. Casazza, C. T. Overton, J. C. Callaway, and J. Y. Takekawa. 2014. Wetland accretion rate model of ecosystem resilience (WARMER) and its application to habitat sustainability for endangered species in the San Francisco Estuary. Estuar. Coasts 37: 476–492, doi:10.1007/s12237-013-9694-0

Syvitski, J. P. M., C. J. Vörösmarty, A. J. Kettner, and P. Green. 2005. Impact of humans on the flux of terrestrial sediment to the global coastal ocean. Science 308: 376–380, doi:10.1126/science.1109454

Temmerman, S., T. J. Bouma, G. Govers, Z. B. Wang, M. B. De Vries, and P. M. J. Herman. 2005. Impact of vegetation on flow routing and sedimentation patterns: Three-dimensional modeling for a tidal marsh. J. Geophys. Res. Earth Surf. 110: F04019, doi:10.1029/2005JF000301

Temmerman, S., T. J. Bouma, J. Van de Koppel, D. Van der Wal, M. B. De Vries, and P. M. J. Herman. 2007. Vegetation causes channel erosion in a tidal landscape. Geology 35: 631–634, doi:10.1130/G23502A.1

Thorne, K. and others. 2018. U.S. Pacific coastal wetland resilience and vulnerability to sea-level

687 rise. Sci. Adv. 4: eaao3270, doi:10.1126/sciadv.aao3270
688 Torio, D. D., and G. L. Chmura. 2013. Assessing coastal squeeze of tidal wetlands. J. Coastal
689 Res. 29: 1049–1061, doi:10.2112/JCOASTRES-D-12-00162.1
690 Valiela, I., J. M. Teal, and N. Y. Persson. 1976. Production and dynamics of experimentally
691 enriched salt marsh vegetation: Belowground biomass[1]. Limnol. Oceanogr. 21: 245–252,
692 doi:10.4319/lo.1976.21.2.0245
693 Vinent, O. D., E. R. Herbert, and M. L. Kirwan. 2019. Lower threshold for marsh drowning
694 suggests loss of microtidal marshes regardless of sediment supply. EarthArXiv,
695 doi:10.31223/OSF.IO/CXVQ6
696 Warren, R. S., and W. A. Niering. 1993. Vegetation change on a Northeast tidal marsh:
697 Interaction of sea-level rise and marsh accretion. Ecology 74: 96–103, doi:10.2307/1939504
698 Watson, E. B., K. Szura, C. Wigand, K. B. Raposa, K. Blount, and M. Cencer. 2016. Sea level
699 rise, drought and the decline of *Spartina patens* in New England marshes. Biol. Conserv.
700 196: 173–181, doi:10.1016/J.BIOCON.2016.02.011
701 Watson, E. B., C. Wigand, E. W. Davey, H. M. Andrews, J. Bishop, and K. B. Raposa. 2017.
702 Wetland loss patterns and inundation-productivity relationships prognosticate widespread
703 salt marsh loss for southern New England. Estuar. Coasts 40: 662–681,
704 doi:10.1007/s12237-016-0069-1
705 Weston, N. B. 2014. Declining sediments and rising seas: An unfortunate convergence for tidal
706 wetlands. Estuar. Coasts 37: 1–23, doi:10.1007/s12237-013-9654-8
707 Wilson, C. A., Z. J. Hughes, D. M. FitzGerald, C. S. Hopkinson, V. Valentine, and A. S. Kolker.
708 2014. Saltmarsh pool and tidal creek morphodynamics: Dynamic equilibrium of northern
709 latitude saltmarshes? Geomorphology 213: 99–115, doi:10.1016/j.geomorph.2014.01.002

Wright, L. D., J. P. M. Syvitski, and C. R. Nichols. 2019. Sea Level Rise: Recent Trends and Future Projections, p. 47–57. In L. Wright and C. Nichols [eds.], Tomorrow's Coasts: Complex and Impermanent. Coastal Research Library vol. 27, Springer.

Wu, W., P. Biber, and M. Bethel. 2017. Thresholds of sea-level rise rate and sea-level rise acceleration rate in a vulnerable coastal wetland. Ecol. Evol. 7: 10890–10903, doi:10.1002/ece3.3550

Zedler, J. B., and S. Kercher. 2005. Wetland resources: Status, trends, ecosystem services, and restorability. Annu. Rev. Environ. Resour. 30: 39–74, doi:10.1146/annurev.energy.30.050504.144248

Zhang, X., N. Leonardi, C. Donatelli, and S. Fagherazzi. 2019. Fate of cohesive sediments in a marsh-dominated estuary. Adv. Water Resour. 125: 32–40, doi:10.1016/J.ADVWATRES.2019.01.003

723 Acknowledgments

724 Conversations with Anne Giblin and Jim Morris helped motivate this work. We thank Jim
725 Morris and James Edwards for providing the DEM and habitat base maps, and Hap Garritt and
726 Tyler Messerschmidt for helping locate public datasets. This work was supported by NSF
727 Coastal SEES (#1426981), NSF LTER (Plum Island Ecosystems #1637630 and Virginia Coast
728 Reserve #1832221), NSF GLD (#1529245), and NSF CAREER (#1654374). The authors have
729 no affiliations with any organizations with financial or non-financial interests in the subject
730 matter discussed in this manuscript and therefore declare no conflict of interest. This is
731 contribution no. 3888 of the Virginia Institute of Marine Science.

732 Table 1. Model parameterization for computing mineral and organic accretion rates

Parameter	Description	Value	Reference
Mineral Accretion (A_m)			
C_0	Suspended sediment concentration	10-20 mg L^{-1}	Hopkinson et al. 2018
w_s	Settling velocity	1 x 10^{-4} m s^{-1}	Temmerman et al. 2005
ρ_m	Inorganic sediment density	1.99 x 10^6 g m^{-3}	Morris et al. 2016
Organic Accretion (A_o)			
P_{SAmax}	*S. alterniflora* maximum biomass	500-1500 g m^{-2}	Morris and Sundberg 2013a; b
P_{SPmax}	*S. patens* maximum biomass	750-1750 g m^{-2}	Morris and Sundberg 2013a; b
B_{SA}	*S. alterniflora* biomass ratio	4.5	
B_{SP}	*S. patens* biomass ratio	1.8	
k	Recalcitrant fraction coefficient	0.1	Benner et al. 1984
ρ_o	Organic sediment density	8.5 x 10^4 g m^3	Morris et al. 2016
Elevation (Z)			
E_{DEM}	Potential DEM error	Z±0.2 m	Edwards 2016

733

734

735 Table 2. Summary of habitat area (mean±1 SD) and percent change in habitat type between 2011
736 and 2100 under historical, medium, and high SLR scenarios (n=300 model runs per scenario)

	2011	Historical 2100		Medium 2100		High 2100	
	km^2	km^2	% change	km^2	% change	km^2	% change
Total marsh	40.7±0.48	42.4±0.28	+4	43.6±0.28	+7	44.2±0.28	+9
Low marsh	7.26±3.72	2.35±0.54	-68	26.4±9.65	+264	40.5±0.35	+458
High marsh	33.4±3.33	40.1±0.46	+20	17.2±9.50	-49	3.70±0.25	-89
Upland	2.40±0.26	2.02±0.13	-16	1.68±0.11	-30	1.33±0.09	-45

737

738

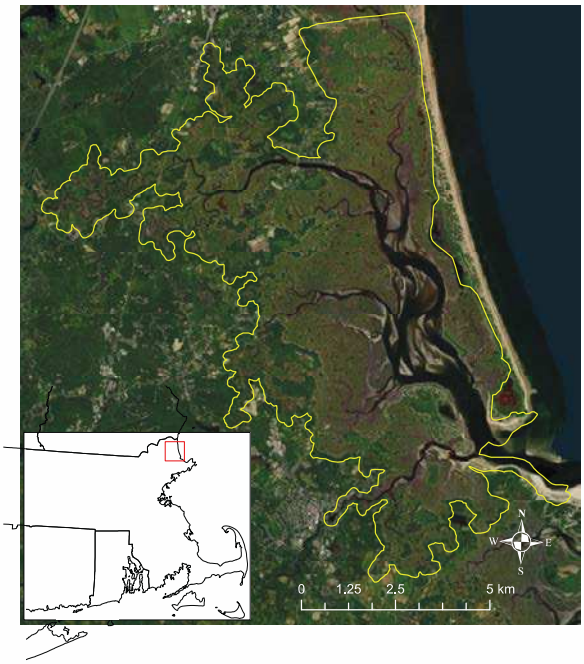

739

740 Figure 1. Location map of Plum Island Ecosystems LTER, Massachusetts, USA.

741

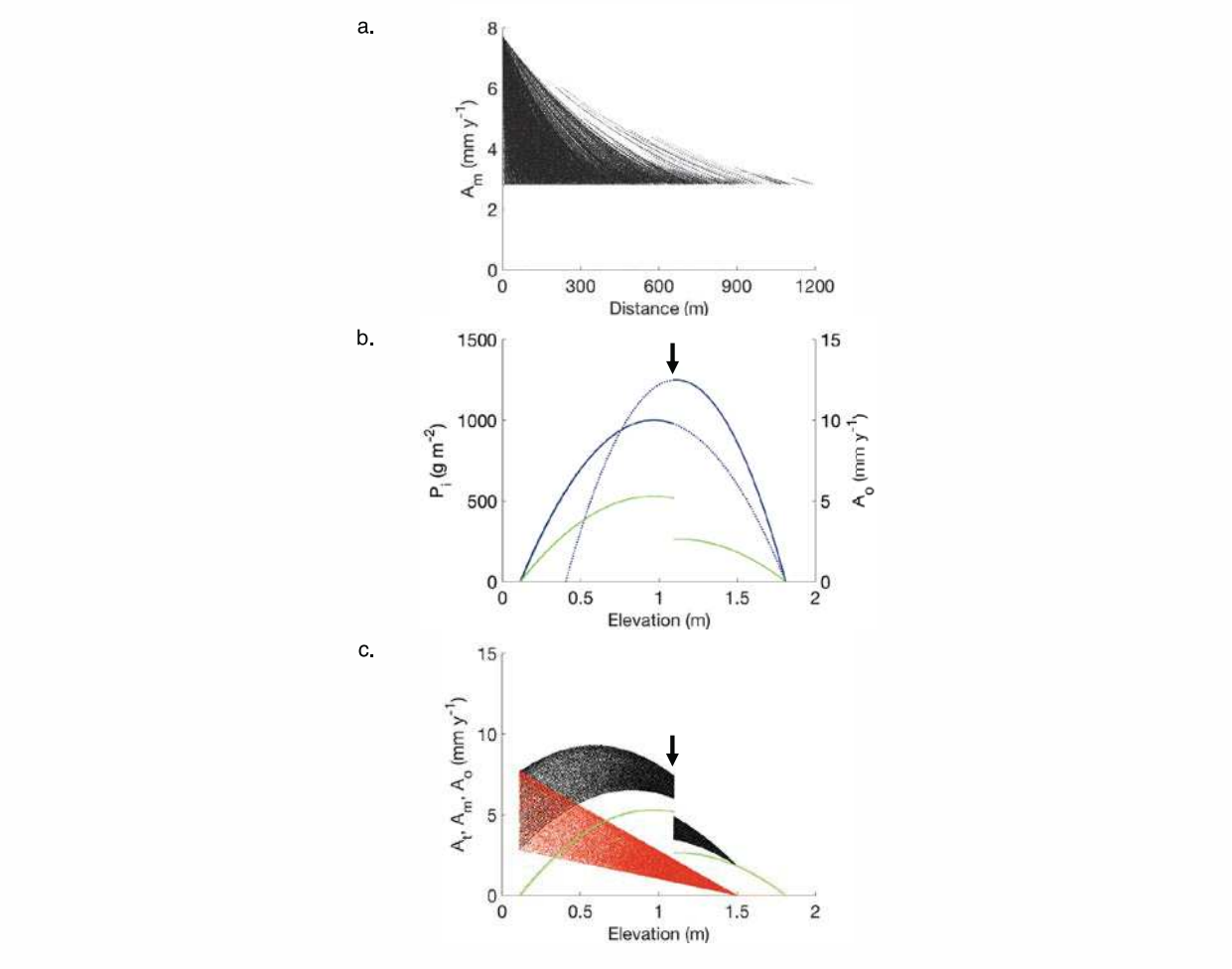

Figure 2. Model design for mineral and organic accretion: a) mineral accretion rates (A_m) decrease with distance from the nearest channel and vary depending on local drainage basin size, illustrated using a constant elevation (z = 0.109 m) across the marsh (grid size: $10m^2$) and initial accretion rates; b) aboveground biomass (P_i: blue) and organic accretion rates (A_o: green) for *Spartina alterniflora* (below 1.09 m) and *S. patens* (above 1.09 m) depend on marsh elevation (arrow marks low to high marsh transition; dotted curve is the portion of the biomass curve outside modeled elevation range for each species); c) total, mineral and organic accretion rates across elevation (A_t: black; A_m: orange; A_o: green) at every position on the marsh under initial conditions; for a given elevation, A_m varies depending on distance from the nearest channel.

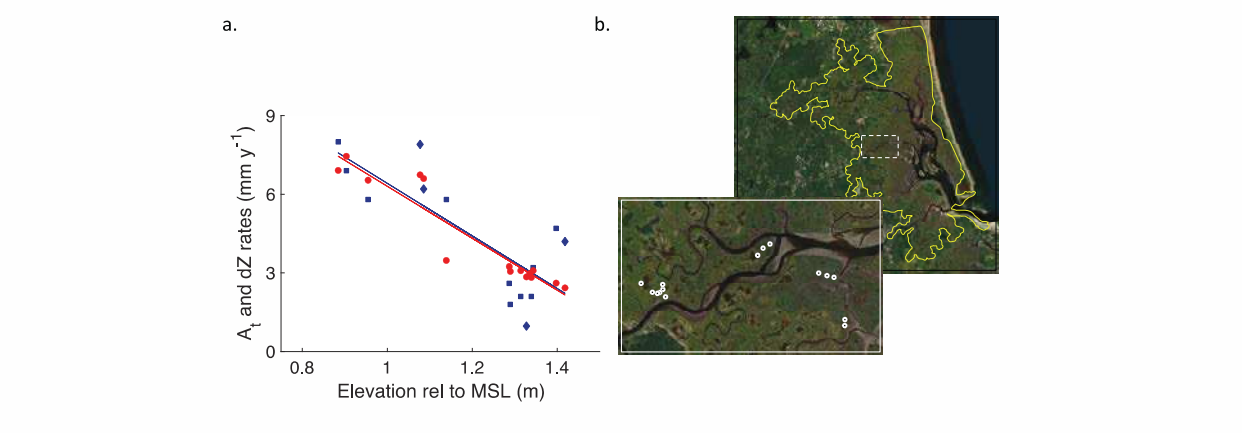

752

753 Figure 3. Model comparison: a) accretion and elevation change rates across elevation (modeled
754 accretion rates: red circles; observed rates of elevation change: blue squares; observed accretion
755 rates: blue diamonds); b) locations of observed rates from SETs and ^{210}Pb cores reported in
756 Wilson et al. 2014.

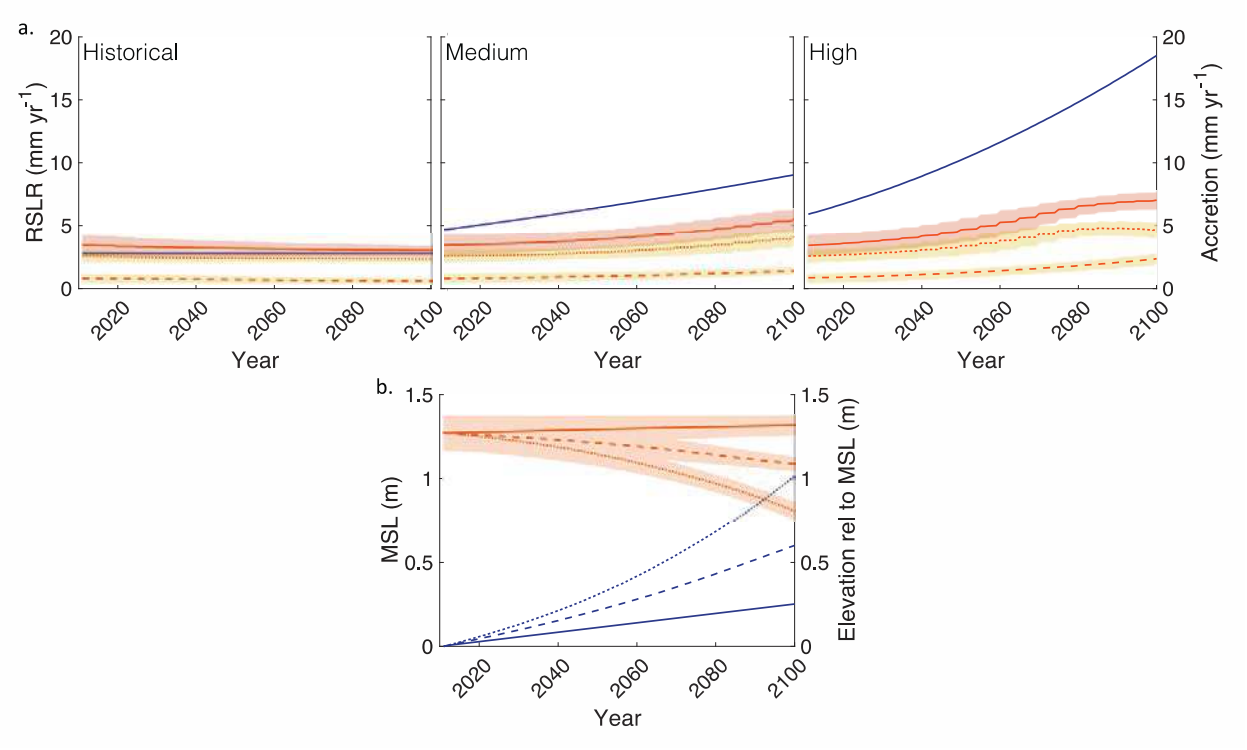

Figure 4. Mean marsh accretion rates (±1 SD) over time a) under the historical, medium, and high SLR scenarios (rate of SLR: blue line; A_t: solid orange; A_m: dashed orange; A_o: dotted orange), and b) mean elevation (orange lines; ±1 SD) and MSL (blue lines) over time for historical (solid), medium (dashed), and high (dotted) SLR scenarios.

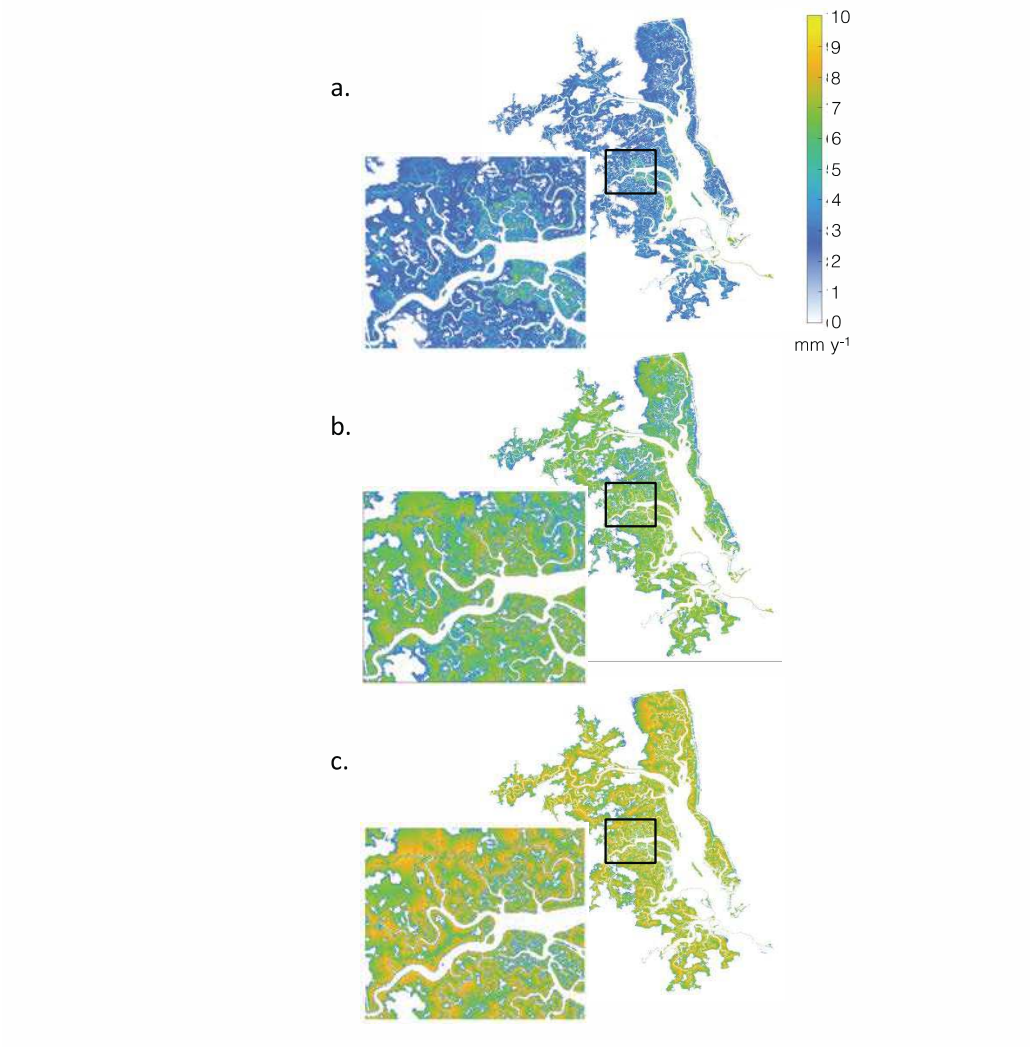

762

763 Figure 5. Total (A_t) accretion rates in 2100 for a) historical, b) medium, and c) high SLR

764 scenarios. Inset highlights portion of PIE dominated by low marsh, where observed accretion and

765 elevation change rates are measured.

766

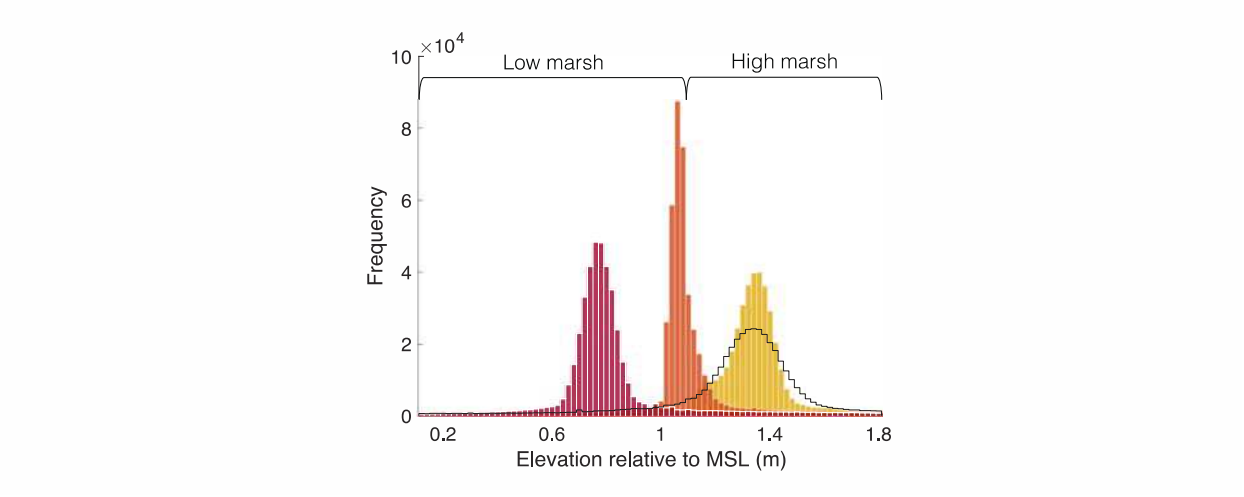

Figure 6. Elevation change for each SLR scenario: elevation distribution across the marsh platform in 2011 (black outline) and in 2100 for historical (yellow), medium (orange), and high (red) SLR scenarios.

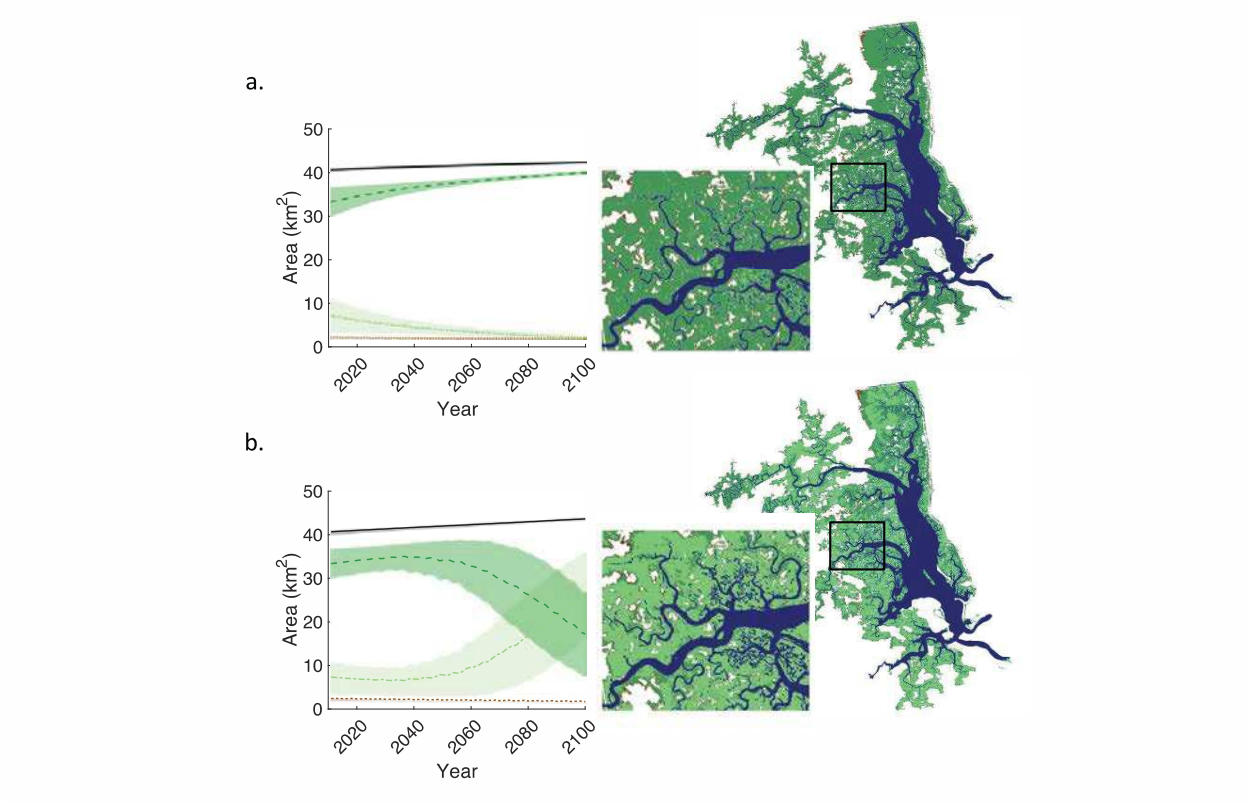

Figure 7. Mean habitat area (±1 SD) over time (total marsh: solid black line; high marsh: dashed green; low marsh: dash-dot yellow; upland: dotted brown) and spatial distribution of habitat in 2100 (high marsh: green; low marsh: yellow; water: blue; upland: brown) for a) historical and b) medium SLR scenarios. Note that white patches are ponds and high elevation areas outside the model domain.

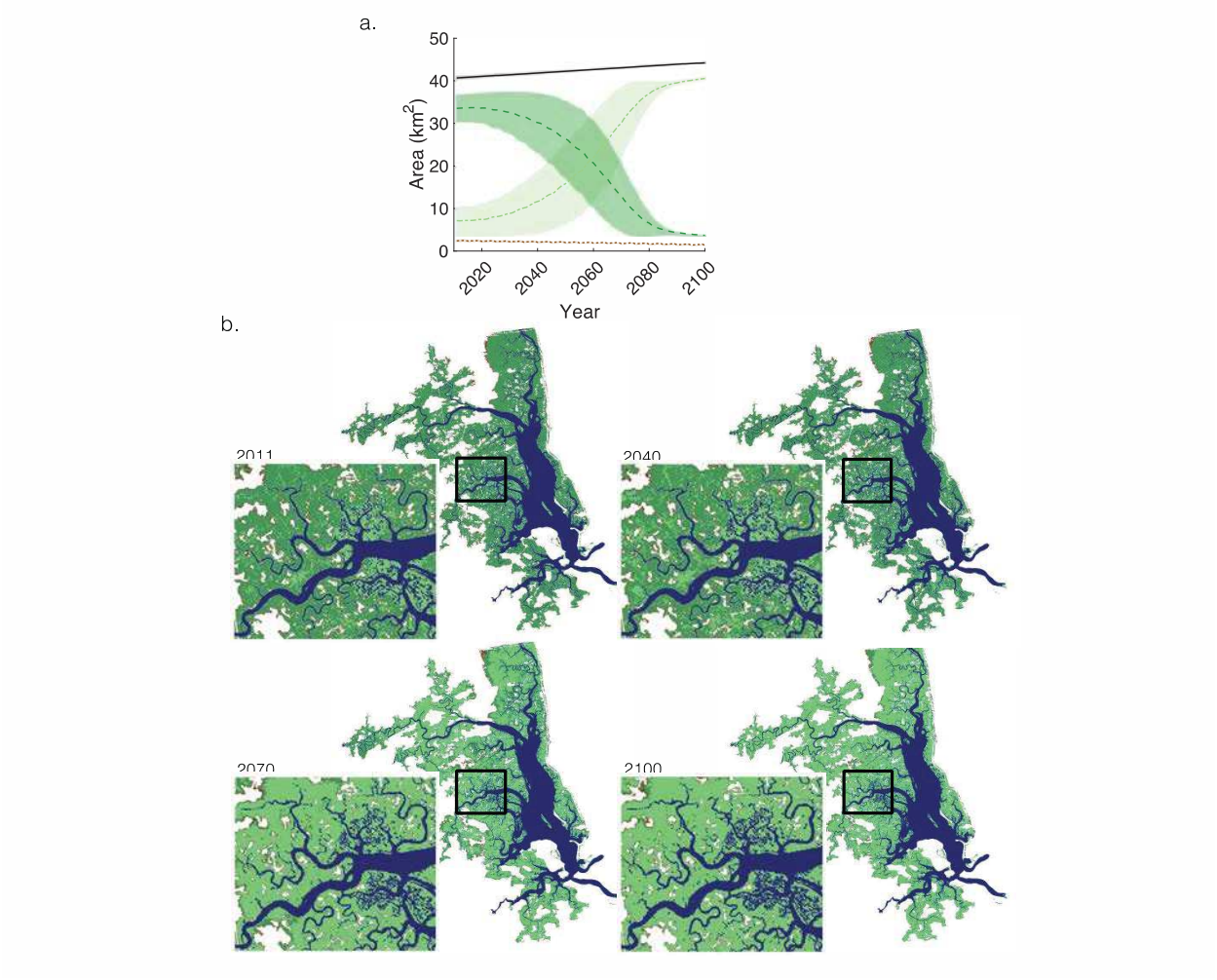

777

778 Figure 8. Habitat changes under the high SLR scenario in a) mean area over time (±1 SD; total
779 marsh: solid black line; high marsh: dashed green; low marsh: dash-dot yellow; upland: dotted
780 brown), and b) spatial distribution in 2011, 2040, 2070, and 2100 (high marsh: green; low marsh:
781 yellow; water: blue; upland: brown).

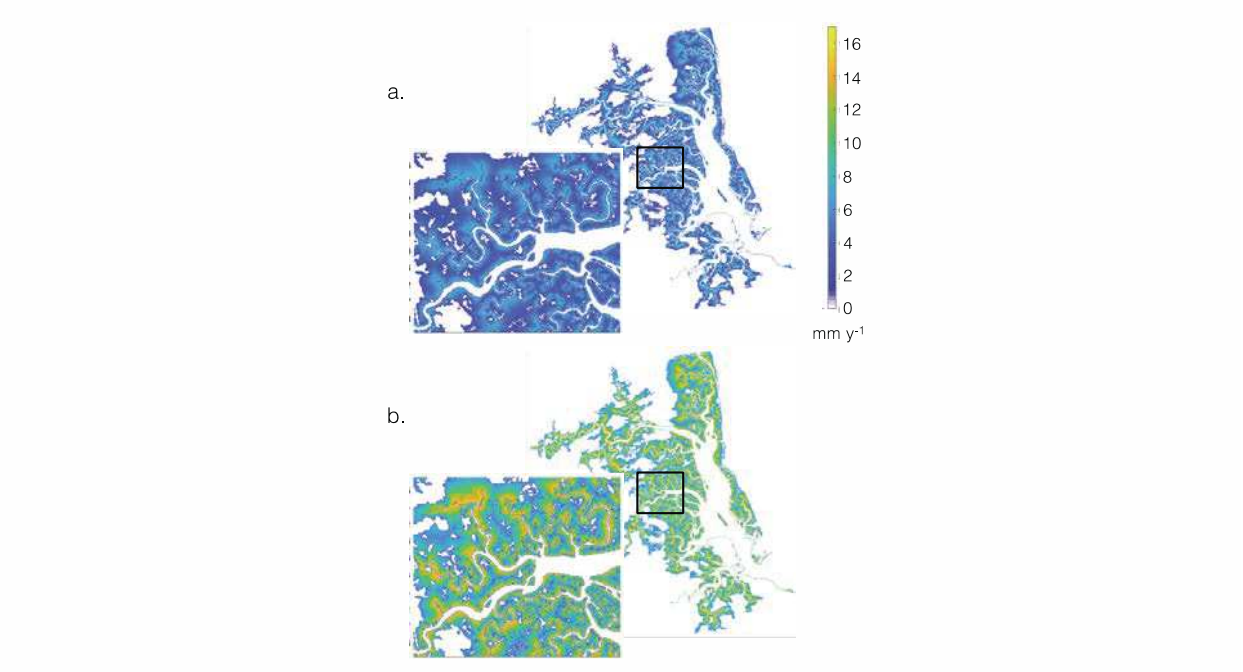

Figure 9. Comparison of maximum mineral accretion rates under a) the current median suspended sediment concentration of 15 mg L^{-1} and b) a hypothetical suspended sediment concentration of 30 mg L^{-1}; elevation in each scenario was set to a uniform depth of 0.109 m above MSL.